



Pergamon

# Characterization of HERG Potassium Channel Inhibition Using CoMSiA 3D QSAR and Homology Modeling Approaches

Robert A. Pearlstein,<sup>a</sup> Roy J. Vaz,<sup>a,\*</sup> Jiesheng Kang,<sup>a</sup> Xiao-Liang Chen,<sup>a</sup>  
Maria Preobrazhenskaya,<sup>b</sup> Andrey E. Shchekotikhin,<sup>b</sup> Alexander M. Korolev,<sup>b</sup>  
Ludmila N. Lysenkova,<sup>b</sup> Olga V. Miroshnikova,<sup>b</sup> James Hendrix<sup>a</sup> and David Rampe<sup>a</sup>

<sup>a</sup>Aventis Pharmaceuticals, 1041 Route 202/206 N, Bridgewater, NJ 08876, USA

<sup>b</sup>Russian Academy of Medical Sciences, Gause Institute of New Antibiotics, Bolshaya Pirogovskaya 11, Moscow 119867, Russia

Received 15 May 2002; accepted 31 October 2002

**Abstract**—A data set consisting of twenty-two sertindole analogues and ten structurally diverse inhibitors, spanning a wide range in potency, was analyzed using CoMSiA. A homology model of HERG was constructed from the crystal structure of the open MthK potassium channel. A complementary relationship between our CoMSiA and homology models is apparent when the long inhibitor axis is oriented parallel to the longitudinal axis of the pore, with the tail region pointed toward the selectivity filter. The key elements of the pharmacophore, the CoMSiA and the homology model are: (1) The hydrophobic feature optimally consists of an aromatic group that is capable of engaging in  $\pi$ -stacking with a Phe656 side chain. Optionally, a second aromatic or hydrophobic group present in some inhibitors may contact an additional Phe656 side chain. (2) The basic nitrogen appears to undergo a  $\pi$ -cation interaction with Tyr652. (3) The pore diameter (12 Å +), and depth of the selectivity loop relative to the intracellular opening, act as constraints on the conformation-dependent inhibitor dimensions.

© 2003 Elsevier Science Ltd. All rights reserved.

The HERG potassium channel (*human ether-a-go-go*-related gene) is expressed in the human heart. The channel is a key effector of cardiac repolarization and contributes to the QT interval measured by the electrocardiogram. Inhibition of HERG can lead to a prolongation of the QT interval, widely considered a critical risk factor for torsades de pointes arrhythmia. Most compounds that prolong the QT interval do so via a specific, high affinity blockade of HERG.<sup>1</sup> Such chemically diverse drugs as terfenadine (Seldane<sup>®</sup>), cispripide (Propulsid<sup>®</sup>), and astemizole (Hismanal<sup>®</sup>)<sup>2</sup> have been withdrawn from the market due to their HERG blocking properties and attending QT interval prolongation. Thus, HERG inhibitory effects represent an important safety consideration in drug discovery. The prevalence of this problem reflects a significant probability of overlap between the HERG pharmacophore and that for many primary target classes. Pharmacophore and QSAR analysis studies have been hampered by the lack of consistent, high quality data sets. Pharmacophore models generated using Catalyst<sup>3</sup> and CoMFA<sup>4</sup> have been reported in the recent literature. *In Silico* profiling

methods have also been proposed for generating biased libraries enriched with non-HERG inhibitors.<sup>5</sup>

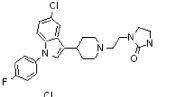
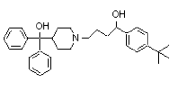
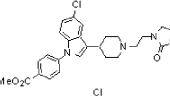
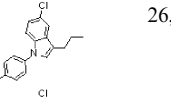
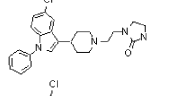
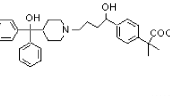
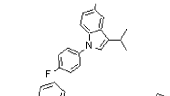
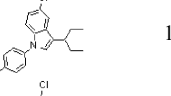
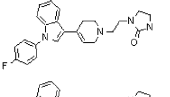
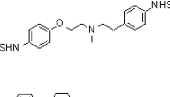
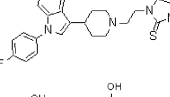
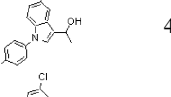
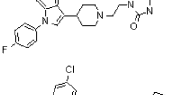
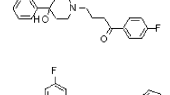
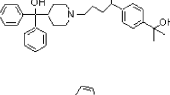
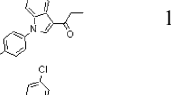
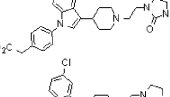
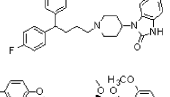
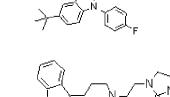
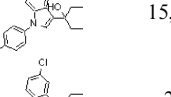
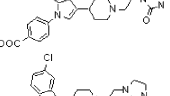
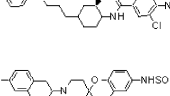
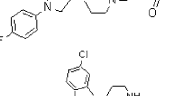
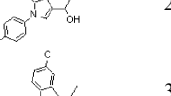
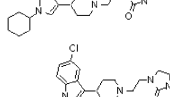
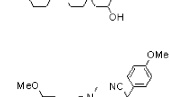
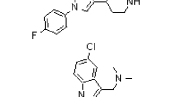
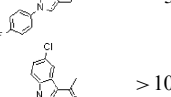
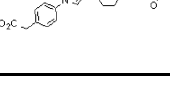
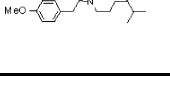
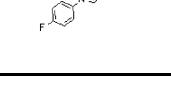
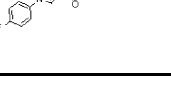
Sertindole, an antipsychotic drug exhibiting high affinity HERG blockade,<sup>6</sup> is a useful starting point for studying HERG structure–activity relationships. The fluorophenyl–piperidyl substituted indole scaffold of sertindole is conformationally constrained,<sup>7</sup> making it an attractive template for structural comparisons with other HERG inhibitors. We probed the possible structural requirements of HERG inhibition by synthesizing a series of sertindole analogues in which structural features were systematically omitted or changed. HERG IC<sub>50</sub> values were determined for these analogues using patch clamp electrophysiology. A comparative molecular similarity analysis (CoMSiA)<sup>8</sup> was performed for the sertindole series together with a diverse set of known inhibitors (see Table 1).

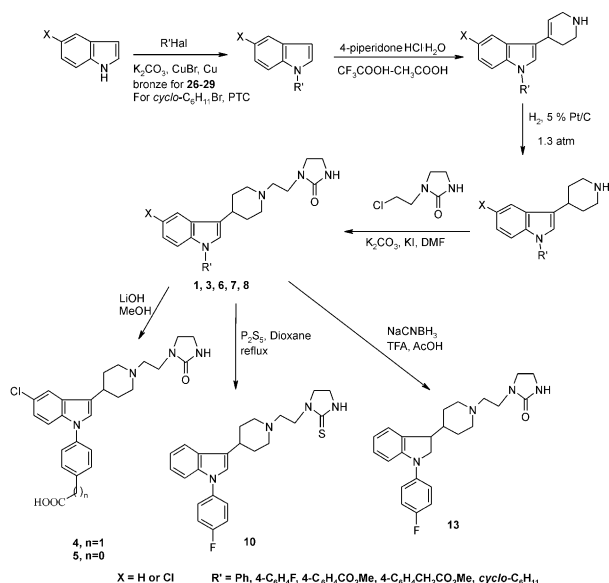
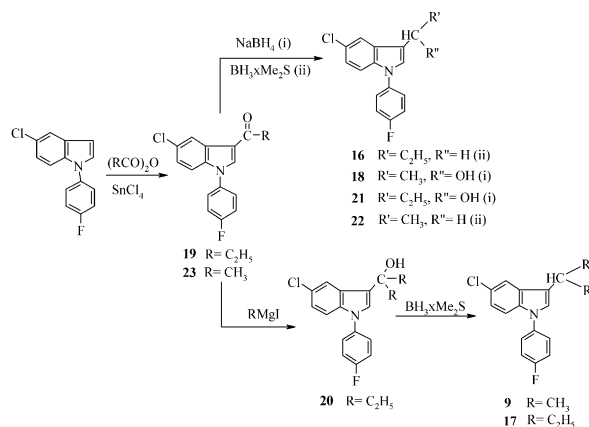
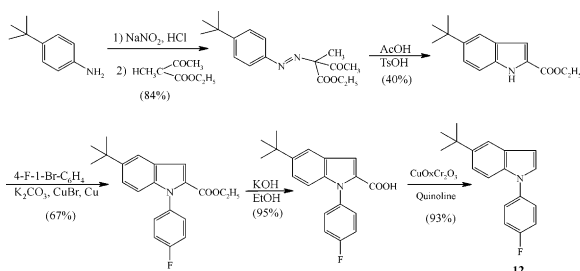
## Synthesis of the Sertindole Analogues

The synthesis schemes for the sertindole analogues listed in Table 1 are reported in Schemes 1–3. Analogues **2**, **3**, and **14** were prepared via the method of Perregaard et

\*Corresponding author. E-mail: roy.vaz@aventis.com

**Table 1.** Structures and their hERG activities used in the analysis (\*ref 15, \*\*ref 16)

Compd	Structure	IC <sub>50</sub> (nM)	Compd	Structure	IC <sub>50</sub> (nM)	Compd	Structure	IC <sub>50</sub> (nM)	Compd	Structure	IC <sub>50</sub> (nM)
sertindole		3	terfenadine		56	<b>8</b>		36	<b>16</b>		26,000
<b>1</b>		88	fexofenadine		23,000	<b>9</b>		> 10,000	<b>17</b>		1480
<b>2</b>		10	dofetilide		10	<b>10</b>		6.2	<b>18</b>		4550
<b>3</b>		7	haloperidol		32	<b>11</b>		460	<b>19</b>		1947
<b>4</b>		579	pimozide		18	<b>12</b>		> 10,000	<b>20</b>		15,700
<b>5</b>		75,000	cisapride		45	<b>13</b>		23.5	<b>21</b>		2200
<b>6</b>		137	MK499		34*	<b>14</b>		204	<b>22</b>		3500
<b>7</b>		131	verapamil		143**	<b>15</b>		11	<b>23</b>		> 10000

Scheme 1. Compounds **1**, **3–8**, **10**, and **13**.Scheme 2. Compounds **9** and **16–23**.Scheme 3. Compound **12**.

al.<sup>9</sup> Compound **11** was prepared via the method of Carr et al.<sup>10</sup> Compound **15** was prepared via the method of Andersen et al.<sup>11</sup>

### HERG channel electrophysiology

Chinese hamster ovary cells stably expressing the HERG cardiac potassium channel were used for these experiments. Standard whole-cell patch clamp electrophysiology was used to record HERG channel currents

from these cells as described previously.<sup>12</sup> All compounds were added to the cells in ascending concentrations, and IC<sub>50</sub> values for HERG channel inhibition were calculated.

### HERG channel 3D-QSAR (CoMSiA) model

A CoMSiA model was constructed using IC<sub>50</sub> values for all but four of the 32 compounds shown in Table 1. Our data set includes our sertindole series and several published structurally diverse chemotypes, which together span a wide range of HERG potency. The superimposed structures of representative compounds included in our CoMSiA model are shown in Figure 4. Four compounds (**1**, **3**, **7**, and **21**) representing the available range in IC<sub>50</sub> were withheld from the CoMSiA training set as a means of validating the prediction accuracy of our model.

Electrostatic calculations have shown that monovalent cations are stabilized within the pore of the KcsA potassium channel,<sup>13</sup> and many potassium channels including HERG are blocked by quaternary alkylamines.<sup>14</sup> Electrophysiological evidence suggests that inhibitors bind within the intracellular lumen of the potassium conduction pore,<sup>15</sup> which is believed to contain a large water-filled cavity. Although important differences<sup>16</sup> between HERG and other potassium channels likely exist, it is reasonable to assume that a preference for cationic species is shared among all potassium channels. Therefore, our conformational energy and CoMSiA calculations were performed using the protonated form of the basic nitrogen, where present. The active conformations of sertindole and MK-499 were reconstructed based on those described previously.<sup>7,15</sup> Conformational searching was performed on all other inhibitors using the MMFF94 force field in vacuum, as implemented in Sybyl 6.7.2 (available from Tripos, Inc., St. Louis, MO). The candidate active conformations were selected from among those within 5 kcal of the lowest minimum energy conformation. The final chosen conformation was that which gave the best correlation in the CoMSiA model. This is particularly evident in the case of terfenadine and its metabolite, fexofenadine.

Two minimum energy conformations are predicted for terfenadine. These are a linear conformation denoted as conf-1 and an intra-molecular H-bond stabilized conformation denoted as conf-2. Conf-2 is the lowest energy conformation, and the only one observed in the crystal structure of the isolated compound (data on file at Aventis Pharmaceuticals, Inc.). Three minimum energy conformations are predicted for fexofenadine (Fig. 1). Two are similar to conf-1 (yellow) and conf-2 (magenta) predicted for terfenadine. The third conformation denoted as conf-3 (cyan) consists of the folded form, which is stabilized by a 'salt bridge' interaction between its carboxylate oxygen and protonated piperdyl nitrogen. This is the lowest energy conformation for fexofenadine, and is observed together with other conformations in the crystal structure of the isolated compound (data on file at Aventis

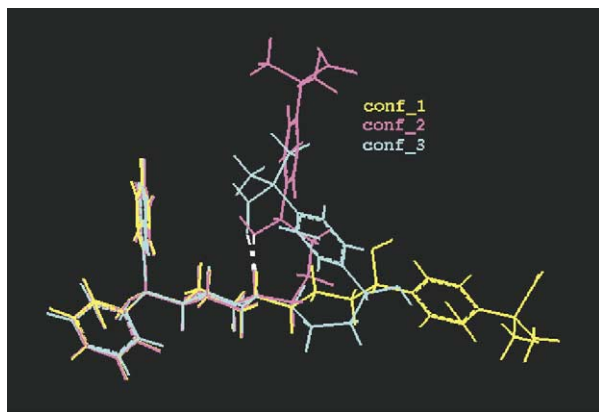


**Figure 1.** Conformations of fexofenadine tested in the CoMSiA models (see text).

Pharmaceuticals, Inc.). This conformation is not accessible to terfenadine, which lacks the carboxyl group. The intra-pore environment is likely to influence inhibitor conformational stability. However, there is no obvious choice of conformational energy calculation conditions (e.g., solvent versus vacuum, dielectric constant) that best approximate this environment. Water and ions present in the pore would likely destabilize the intra-molecular hydrogen bond in conf-2. The carboxylate group in conf-1 of fexofenadine likely requires an inter-molecular counter-ion partner, which is unlikely to exist based on the predicted hydrophobic side chain composition of the pore lining (see the next section). Environmental considerations are thus suggestive of conf-1 and conf-3 as the active conformations of terfenadine and fexofenadine, respectively. CoMSiA models were constructed by incorporating different permutations of conf-1, conf-2, and conf-3 for each analogue. The statistics for the models are listed in Table 2. The model with the largest  $q^2$  (see the bold entry in Table 2) is obtained for conf-1 and conf-3 of terfenadine and fexofenadine, respectively. The non-folded fexofenadine conformations (conf-1 or conf-2) result in models with much lower statistical validity. Our CoMSiA results provide indirect evidence that the intra-molecular salt bridge-stabilized conformation (conf-3) persists under biological conditions, and that the large difference in HERG channel activity observed between the two analogues can be largely explained in terms of conformational differences.

The centroids of the indole-phenyl and *N*-phenyl rings, nitrogen atoms, and *N*-protons (where existing) were

**Table 2.** Values of  $q^2$  from various CoMSiA trials, using combinations of conformations of terfenadine and fexofenadine. The combination with the best  $q^2$  was used in the final model

Conf of terf	Conf of fexo	$q^2$	SDEP	Components
conf-1	conf-1	0.424	1.034	3
conf-1	conf-2	0.514	0.949	3
<b>conf-1</b>	<b>conf-3</b>	<b>0.571</b>	<b>0.892</b>	<b>3</b>
conf-2	conf-1	0.398	1.08	4
conf-2	conf-2	0.313	1.085	1
conf-2	conf-3	0.481	1.003	3

used as landmarks for superimposing the compounds onto sertindole using least-squares fitting. All compounds in our data set contain at least two of these landmarks. In cases where more than one superposition mode is possible, all were tried and the possibility with the higher  $q^2$  was retained in the model. Our CoMSiA results are based on steric and electrostatic fields. H-bond and hydrophobic CoMSiA fields, with or without steric and electrostatic fields, did not result in increased statistical significance of the model. This is consistent with the non-orthogonality between the hydrophobic/H-bond fields and the steric/electrostatic fields.

The CoMSiA models are based on 470 grid points with a 2 Å separation and a minimum sigma of 2.0 kcal. Plots of fitted versus actual  $\text{pIC}_{50}$  ( $-\log\text{IC}_{50}$ ) are provided in Figure 2. The statistics of the model are shown in Figure 3. The four compounds omitted from the training set are shown as red points. The predicted values of these compounds fall well within the standard errors of the fitted model.

The negative steric contour shown in red in Figure 4 corresponds to a (S.D.) times (coeff.) (referred to subsequently as coefficients) of  $-0.005$ . This contour level encompasses the region of fexofenadine that differentiates it from terfenadine. Substituents on the hydrophobic groups corresponding to the indole phenyl and *N*-phenyl rings of sertindole are also covered by this contour. The addition of steric bulk to these regions is predicted to reduce HERG activity. The  $+0.005$  steric contour shown in green in Figure 4 encompasses the entire central inhibitor region and that corresponding to the *N*-phenyl ring of sertindole. The hydrophobic feature corresponding to the *N*-phenyl ring of sertindole is present in a subset of inhibitors, providing an opportunity for variance in this region to contribute to the correlation. On the other hand, co-variance between the fields and activities cannot be observed in the region corresponding to the indole phenyl ring of sertindole

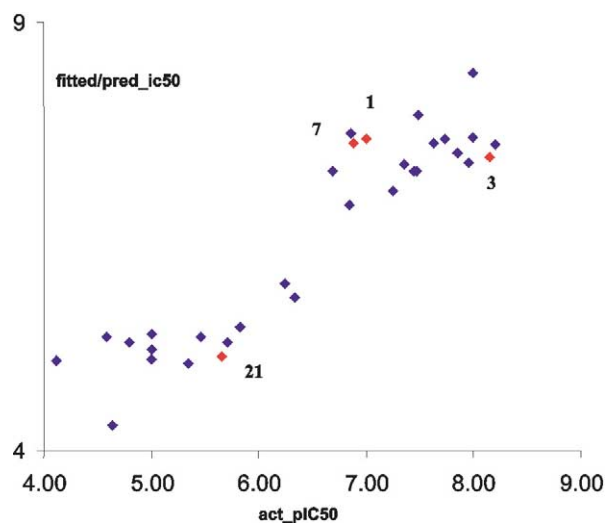


**Figure 2.** Fitted (blue) and predicted (red)  $\text{pIC}_{50}$  values for the studied compounds. The predicted compounds (withheld during CoMSiA model construction) fall well within the fitted set of compounds.



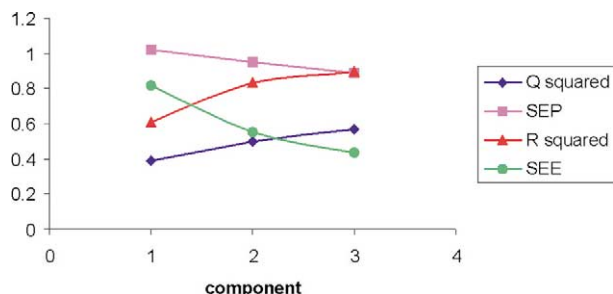


**Figure 3.** Statistical parameters  $q^2$ ,  $r^2$ , standard error of prediction (SEP) and Standard Error of Estimate (SEE) from the PLS model.

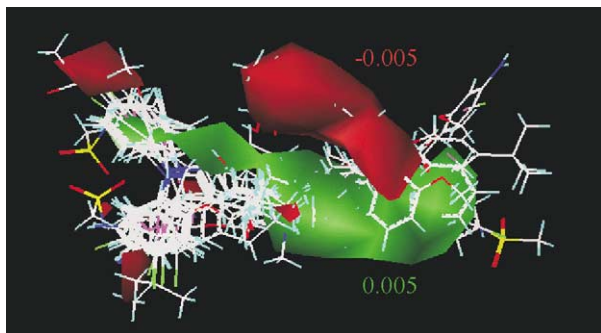


**Figure 4.** Superposition of the studied compounds showing the steric coefficients (coefficient values =  $\pm 0.005$ ) from the CoMSiA. The contours of coefficients corresponding to the red region suggest desirable substitution sites aimed at decreasing HERG affinity.

due to the absence of inhibitors lacking this feature in the data set. On the basis of the absence of such inhibitors, it is reasonable to conclude that this hydrophobic feature is required for activity and is implicitly present in the CoMSiA model. The 0.02 electrostatic coefficient contour level shown in orange in Figure 5 overlaps with the basic nitrogen feature. A positive correlation between HERG activity and 'increased' positive charge in this region is predicted. The other positive coefficient contour is due to the acid group on compounds **4** and **5**, which when neutralized by esterification in compounds **7** and **8** respectively, results in increased inhibitory activity. The electrostatic coefficients contribute 76% to the CoMSiA model.

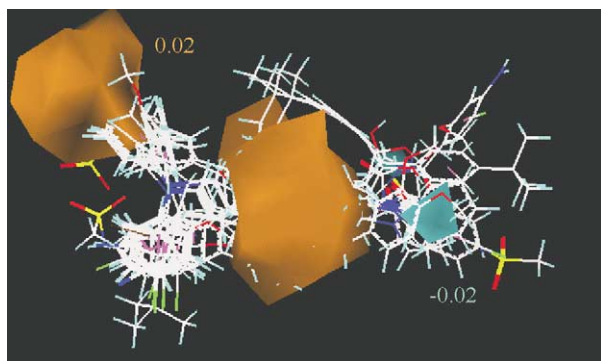


**Figure 5.** Superposition of the studied compounds showing the electrostatic contours of coefficients (coefficient values =  $\pm 0.02$ ) from the CoMSiA. Modifications aimed at increasing the negative charge in the orange regions and the positive charge in the cyan region are predicted to decrease HERG affinity.

The structure–activity relationships of our sertindole series suggest that the HERG binding site is highly tolerant to large changes in the parent compound. Significant potency is retained in analogues lacking the ethyl cyclic urea tail group (compound **14**) or containing a partial piperidyl ring (compound **15**). Complete loss of activity occurs for only three highly truncated analogues (compounds **9**, **12**, and **23**).

### Structure-based interpretation of the CoMSiA model

There is ample evidence in the literature that HERG blockade by small molecules is caused by direct occupation of the pore.<sup>16–18</sup> A crystal structure of the open bacterial MthK potassium channel was recently published.<sup>6</sup> We wanted to explore whether this structure could be used to interpret and refine our CoMSiA-based pharmacophore model. This work was intended to address the following key issues: (1) orientation of the pharmacophore in the binding site; (2) protein partners associated with the proposed pharmacophore features and the nature of the interactions; (3) reported sensitivity differences of mutated forms of HERG to terfenadine, cisapride, and MK-499.

A homology model of the tetrameric pore region of hERG (inner and pore helices and selectivity loop) was constructed from the MthK template and the reported HERG-MthK sequence alignment<sup>17</sup> using Modeler (available from Accelrys, San Diego, CA). The side chains of the MthK pore domain were not resolved in the crystal structure, and were therefore modeled *ab initio*. Complete 4-fold symmetry in the resulting homology model was not obtained due to a slight asymmetry in one of the monomers of the MthK structure. This was particularly apparent for the side chain conformations of Phe656 and Tyr652. The conformations of these side chains were therefore adjusted in our model by copying all corresponding side chain torsion angles from the opposite monomer. Due to the low resolution of the MthK structure and the uncertain structural relationship between the MthK and HERG channels, our homology model should be considered highly qualitative.

The homology model suggests that the lumen of the pore consists of two layers of aromatic side chains contributed by Phe656 and Tyr652. We qualitatively docked the set of aligned inhibitor structures into the homology model. The best correspondences between pharmacophore and pore features were achieved using the following criteria: (1) orientation of the inhibitor long axis parallel to the pore axis, such that the hydrophobic feature(s) are located at the intracellular mouth, and the tail region points toward the selectivity loop. This results in spatial registration between the hydrophobic and basic nitrogen features proposed from our CoMSiA model (6–8 Å separation) with Phe656 and Tyr652 side chains, respectively. (2) Overall shape complementarity between pore and inhibitor surfaces based on graphical visualization using Molcad (available from Tripos). The inhibitor dimensions are qualitatively consistent with the pore diameter (12 Å +) and depth of the

selectivity loop relative to the intracellular opening (spatial constraints).

The proposed binding mode suggests an extended interpretation of our CoMSiA model: (1) the hydrophobic features optimally consist of an aromatic group that is capable of engaging in  $\pi$ -stacking with a Phe656 side chain. Optionally, a second aromatic or hydrophobic group present in some inhibitors may contact a different Phe656 side chain. (2) The basic nitrogen is proposed to undergo a  $\pi$ -cation interaction<sup>19</sup> with Tyr652. The variation in basicity of this feature across the studied inhibitors is suggestive of a  $\pi$ -cation versus salt bridge interaction, which would preferentially involve a tertiary nitrogen. Though not present in our data set, inhibitors that contain a hydrophobic or aromatic group in this position could theoretically engage Tyr652 in hydrophobic or  $\pi$ -stacking interactions in lieu of a  $\pi$ -cation interaction. (3) The tail region occupies the pore between Tyr652 and the selectivity filter in our docking model. This region is structurally and conformationally diverse, and extends maximally to the selectivity loop. The tail region may provide additional interaction sites with the pore lining that are not apparent from our general CoMSiA model. As such, this region may enhance the overall occlusion of the pore. Structure–activity relationships about the tail region are difficult to assess due to its greater diversity and flexibility compared to the other regions. Our sertindole analogues were largely aimed at exploring the structure–activity relationships about this region. Surprisingly, complete removal of the piperdyl *N*-substituent results in significant retention of activity (3–200 nM IC<sub>50</sub>). The importance of the tail region to HERG binding affinity should be considered on a case-by-case basis. We believe that this region is best addressed via ‘local’ pharmacophore models derived for individual series of interest incorporating variation in the tail region.

Phe656 and Tyr652 were shown via site-directed mutagenesis to promote sensitivity of HERG to inhibition by MK-499, terfenadine, and cisapride.<sup>15,18</sup> However, only MK-499 blockade demonstrated sensitivity to mutation of Val625. The alignment and conformations predicted from our CoMSiA model suggest that the methylsulfonamide group of MK-499 lies in a region that is not occupied by terfenadine and cisapride. Furthermore, the methylsulfonamide group is spatially close to Val625 in the docked model (Fig. 6). The Val625Ala mutation may eliminate a possible van der Waals interaction with MK-499 that does not occur for terfenadine or cisapride. Recent evidence suggests that altering the relative positions of Phe656 and Tyr652 via mutagenesis results in decreased sensitivity to cisapride.<sup>18</sup> This further supports our proposed CoMSiA-homology model relationships.

HERG contains a promiscuous binding site for drug-like molecules. This can be explained partly by the large volume of the binding site and partly by the nature of the pharmacophore. Our results suggest that diverse inhibitor chemotypes can be described by a somewhat

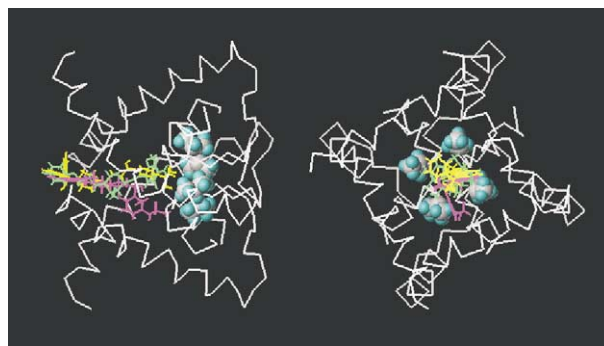


**Figure 6.** Orthogonal views of terfenadine (yellow), cisapride (green), and MK-499 (magenta) docked into the homology model of HERG. MK-499 is predicted to approach closer to Val625 (in spacefill) which showed decreased affinity for Val625Ala. Our model suggests a possible interaction with Val625 that may be unique among the three compounds.

variable set of pharmacophore feature types having a relatively constant, well-defined spatial relationship. For example, the basicity of the nitrogen can vary within the context of a  $\pi$ -cation interaction. It is conceivable that an aromatic or hydrophobic group at this position could also interact with Tyr652 via  $\pi$ - $\pi$  or hydrophobic mechanisms. Compounds **14** and **15** of our sertindole series, which exhibit nanomolar potency in the absence of the ethyl cyclic urea substituent, suggest that the tail region can be less important than other features of the pharmacophore.

A ‘drain plug’ picture of HERG channel inhibition emerges from our modeling studies. The drain plug shape is complementary to the cylindrical architecture of the pore, with key interaction sites on the drain plug ‘handle’ [aromatic feature(s)] and along the length of the plug (basic nitrogen and polar group). The depth of penetration can vary, depending on the length of the tail region, maximally extending to the intracellular end of the selectivity filter. The scope of our model is surprising in light of the complexity of the HERG channel. Possibilities for additional binding modes not covered by our model are entirely plausible given the complexity of the protein, its state-dependent conformational changes, and its interactions with the membrane and regulatory proteins. Furthermore, such factors as membrane permeation required for accessing the intra-cellular lumen of the channel and possible shifts in local pK<sub>a</sub> due to changes in membrane potential further complicate the problem of predicting HERG channel inhibitory activity. Nevertheless, it is hoped that our model can be used as a roadmap for explaining HERG channel liabilities in early lead candidates as well as for designing out properties that promote HERG channel binding in such compounds.

## References and Notes

1. Brown, A. M.; Rampe, D. *Pharmaceutical News* **2000**, 7, 15.
2. (a) Roy, M.-L.; Dumaine, R.; Brown, A. M. *Circulation* **1996**, 94, 817. (b) Rampe, D.; Roy, M.-L.; Dennis, A.; Brown, A. M. *FEBS Lett.* **1997**, 417, 28. (c) Zhou, Z.; Vorperian,

- V. R.; Gong, Q.; Zhang, S.; January, C. Y. *J. Cardiovasc. Electrophysiol.* **1999**, *10*, 836.
3. Ekins, S. L.; Crumb, W. J.; Sarazan, R. D.; Wikel, J. H.; Wrighton, S. A. *J. Pharmacol. Exp. Ther.* **2002**, *301*, 427.
4. Cavalli, A.; Poluzzi, E.; De Ponti, F.; Racanatini, M. *J. Med. Chem.* **2002**, *45*, 3844.
5. Roche, O.; Trube, G.; Zuegge, J.; Pflimlin, P.; Alanine, A.; Schneider, G. *ChemBioChem.* **2002**, *3*, 455.
6. Rampe, D.; Murawsky, M. K.; Grau, J.; Lewis, E. W. *J. Pharmacol. Exp. Ther.* **1998**, *286*, 788.
7. (a) Andersen, K.; Liljefors, T.; Hyttel, J.; Perregaard, J. *J. Med. Chem.* **1996**, *39*, 3723. (b) Anderson, K.; Liljefors, T.; Gundertofte, K.; Perregaard, J.; Bogeso, K. P. *J. Med. Chem.* **1994**, *37*, 950.
8. (a) Klebe, G.; Abraham, U.; Mietzner, T. *J. Med. Chem.* **1994**, *37*, 4130. (b) Cramer, R. D., III; Patterson, D. E.; Bunce, J. D. *J. Am. Chem. Soc.* **1988**, *110*, 5959. (c) Cramer, R. D. III; DePriest, S. A.; Patterson, D. E.; Hecht, P. In *3-D QSAR in Drug Design*; Kubinyi, H., Ed.; ESCOM, Leiden, 1993; pp 443. (d) Klebe, G. In *3-D QSAR in Drug Design*; Kubinyi, H.; Folkers, G.; Martin, Y. C. Eds.; Kluwer Academic: Great Britain, 1998; Vol. 3, p 87.
9. Sertindole analogues **2**, **3**, and **14** were prepared via the method of Perregaard et al. Perregaard, J.; Arnt, J.; Boegesoe, K. P.; Hyttel, J.; Sanchez, C. *J. Med. Chem.* **1992**, *35*, 1092.
10. Compound **11** was prepared via the method of Carr et al. Krauss, R. C.; Strom, R. M.; Scortichini, C. L.; Kruper, W. J.; Wolf, R. A.; Carr, A. A.; Rudisill, D. E.; Panzone, G.; Hay, D. A.; Wu, W. W. WO 9500480, 1995.
11. Compound **15** was prepared via the method of Andersen et al. Andersen, K.; Perregaard, J.; Liljefors, T.; Hyttel, J. *J. Med. Chem.* **1996**, *39*, 3723.
12. Kang, J.; Wang, L.; Cai, F.; Rampe, D. *Eur. J. Pharmacol.* **2000**, *392*, 137.
13. Roux, B.; MacKinnon, R. *Science* **1999**, *285*, 100.
14. (a) Suessbrich, H.; Schonherr, R.; Heinemann, S. H.; Lang, F.; Busch, A. *FEBS Lett.* **1997**, *414*, 435. (b) Tamargo, J. *Jpn. J. Pharmacol.* **2000**, *83*, 1.
15. Mitcheson, J. S.; Chen, J.; Lin, M.; Culberson, C.; Sanguinetti, M. C. *Proc. Natl. Acad. Sci. U.S.A.* **2000**, *97*, 12329.
16. Keating, M. T. K.; Sanguinetti, M. C. *Cell* **2001**, *104*, 569.
17. (a) Jiang, Y.; Lee, A.; Chen, J.; Cadene, M.; Chait, B. T.; MacKinnon, R. *Nature* **2002**, *417*, 515. (b) Jiang, Y.; Lee, A.; Chen, J.; Cadene, M.; Chait, B. T.; MacKinnon, R. *Nature* **2002**, *417*, 523.
18. Chen, J.; Seeböhm, G.; Sanguinetti, M. *Proc. Natl. Acad. Sci. U.S.A.* **2002**, *99*, 12461.
19. Zhong, W.; Gallivan, J. P.; Zhang, Y.; Li, L.; Lester, H.; Dougherty, D. A. *Proc. Natl. Acad. Sci. U.S.A.* **1998**, *95*, 12088.